IET Nanobiotechnology

Research Article

IET Journals
The Institution of Engineering and Technology

High-efficiency Ni^{2+}-NTA/PAA magnetic beads with specific separation on His-tagged protein

ISSN 1751-8741
Received on 6th August 2019
Revised 24th September 2019
Accepted on 27th September 2019
E-First on 12th November 2019
doi: 10.1049/iet-nbt.2019.0271
www.ietdl.org

Wenjing Wang[1,2,3,4], Fengzhen Zhou[1,2,3,4], Xiyao Cheng[1,2,3,4], Zhengding Su[1,2,3,4], Huiling Guo[1,2,3,4] ✉

[1]*Key Laboratory of Fermentation Engineering (Ministry of Education), Wuhan 430068, People's Republic of China*
[2]*Hubei Provincial Cooperative Innovation Center of Industrial Fermentation, Wuhan 430068, People's Republic of China*
[3]*National '111' Center for Cellular Regulation and Molecular Pharmaceutics, Wuhan 430068, People's Republic of China*
[4]*Hubei Key Laboratory of Industrial Microbiology, Hubei University of Technology, Wuhan 430068, People's Republic of China*
✉ *E-mail: 405530371@qq.com*

Abstract: To effective capture and universal enrichment of His-tagged protein, polyacrylic acid (PAA) brushes were used to encapsulate Fe_3O_4 nanoparticles, connect NTA, and Ni^{2+} to prepare magnetic beads. These materials provide many advantages, such as excellent stability, tuneable particle size, and a surface for further functionalisation with biomolecules. His-tagged green fluorescence protein (GFP) was separated efficiently, and the binding capacity of Fe_3O_4/MPS@PAA/NTA-Ni^{2+} was 93.4 mg/g. Compared with High-Affinity Ni-NTA Resin and Ni-NTA Magnetic Agarose Beads, Fe_3O_4/MPS@PAA/NTA-Ni^{2+} nanocomposites exhibited higher separation efficiency and binding capacity towards His-tagged GFP. Moreover, the selectivity and recyclability of them for the target proteins were maintained well after six cycles. This study would widen the application of PAA in constructing multifunctional nanocomposites for biomedical fields.

1 Introduction

Proteins are crucial components that makeup all the cells and tissues of the body. They have an important potential for understanding the structure, function, and regulation of tissues and organs [1]. Therefore, the development of efficient protein isolation and purification from a biological source is of great importance for proteomic analysis. Many target proteins are normally expressed as markers for affinity separation, for example histidine-tagged (His-tagged) proteins are widely used [2, 3]. Currently, immobilised metal-ion affinity chromatography (IMAC) is an available method for protein isolation and purification. This method employs the specific affinity between metal ions and amino acid residues [4, 5]. However, it has some limitations, such as its tedious operation, long separation time, the nickel leakage, less efficiency for low-abundance proteins, which limits the application [3, 6–9].

Magnetic nanoparticles have unique advantages in simple operation, fast separation, and high throughput, thus opening a new window for protein purification [10]. To develop functional magnetic nanoparticles for protein purification, many efforts have been made recently [11–14]. Especially, the key to rapid separation of target proteins is to couple the suitable affinity agents on the surface of magnetic nanoparticles [15]. Zou *et al.* [14] successfully synthesised Fe_3O_4/Cys-Ni^{2+} nanoparticles for rapid enrichment and purification of His-tagged proteins directly from the mixture of lysed cells without pretreatment. Hwang *et al.* [16] synthesised Fe_3O_4 nanoparticles functionalised with Zn-DPA ligands for specifically enriching phosphoproteins from complex cell and tissue lysates. Li *et al.* [9] synthesised hierarchical Fe_3O_4@Cu-apatite nanoparticles for enrichment and magnetic separation of His-tagged proteins directly from the mixture of lysed cells with high binding ability. Zhou *et al.* [17] prepared Fe_3O_4/PMG/IDA-Ni^{2+} nanoparticles as affinity probes for separation and purification of His-tagged hSOD1. However, these approaches may have different major drawbacks, such as multi-step reactions, low stability, poor recyclability, and low metal doping. Thus, the effective capture and universal enrichment of His-tagged proteins from complex mixtures remain a significant challenge.

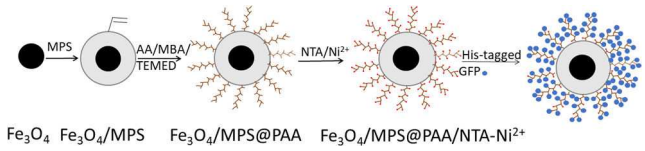

Fig. 1 *Synthetic route of the Fe_3O_4/MPS@PAA/NTA-Ni^{2+} nanocomposites and protein binding to these beads*

To improve the separation efficiency of magnetic beads in protein separation and identification, we synthesised polyacrylic acid (PAA) brushes functionalised Fe_3O_4 nanoparticles for conjugation with Ni^{2+}-NTA (N, N-Bis(carboxymethyl)-L-lysine) to enhance the binding sites (Fig. 1). Specifically, the synthesis procedure involves (i) preparation of Fe_3O_4 cores by a modified solvothermal reaction; (ii) preparation of PAA brushes magnetic core–shell nanocomposites; (iii) conjugation of NTA by EDC/NHS methods and immobilisation of Ni^{2+} on the surface of the nanoparticles. The synthesis of magnetic nanocomposites was characterised by Transmission Electron Microscope (TEM), Dynamic Light Scattering (DLS), Fourier Transform infrared spectroscopy (FTIR), conductivity meter, X-ray Diffraction (XRD), and Vibrating Sample Magnetometer (VSM). Furthermore, the application for selective binding and magnetic separation of His-tagged green fluorescence protein (GFP) from cell lysate was investigated (Fig. 2). Fe_3O_4/MPS@PAA/NTA-Ni^{2+} magnetic nanocomposites showed excellent performance in enrichment and separation of His-tagged GFP.

2 Experimental

2.1 Materials

Ferric chloride hexahydrate ($FeCl_3 \cdot 6H_2O$), ammonium acetate (NH_4Ac), ethylene glycol (EG), ethanol, sodium citrate, nickel (II) chloride hexahydrate ($NiCl_2 \cdot 6H_2O$), ammonium hydroxide (25%), acrylic acid (AA), disodium hydrogen phosphate dodecahydrate ($Na_2HPO_4 \cdot 12H_2O$), imidazole (99%), sodium dihydrogen phosphate dihydrate ($NaH_2PO_4 \cdot 2H_2O$), sodium chloride (NaCl), ammonium persulfate (APS) were purchased from Sinopharm

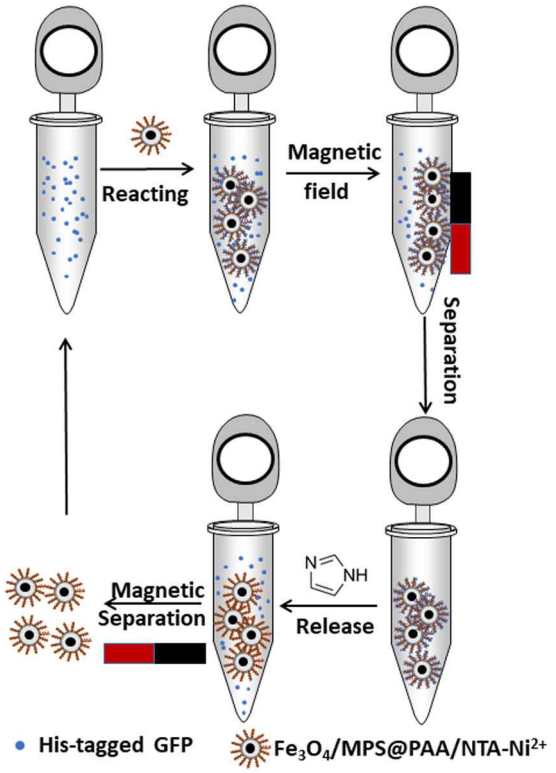

Fig. 2 *Process diagram of the detailed selective purification process for the His-tagged proteins using Fe_3O_4/MPS@PAA/NTA-Ni^{2+} nanocomposites*

Chemical Reagent Beijing Co., Ltd. 3-Methacryloxypropyltrimethoxysilane (MPS), N,N,N′,N′-Tetramethylethylenediamine (TEMED), N-Hydroxysuccinimide (NHS), N,N′-methylenebis (acrylamide) (MBA) were bought from Shanghai Aladdin Biochemical Technology Co., Ltd. N,N-Bis(carboxymethyl)-L-lysine (NTA) was purchased from Shanghai Jizhi Biochemical Technology Co., Ltd. 1-Ethyl-3-(3-dimethyllaminopropyl)carbodiimide hydrochloride (EDC·HCl) was purchased from Shanghai Medpep Co., Ltd. His-tagged GFP was kindly provided by Prof. Zhengding Su (School of Bioengineering and Food, Hubei University of Technology). High-Affinity Ni-NTA Resin and Ni-NTA Magnetic Agarose Beads were purchased from GenScript (Nanjing, China) and Jintai Hongda Biological Technology Co., Ltd. (Beijing, China), respectively. Deionised water used for all experiments was obtained from a Milli-Q system (Millipore, Bedford, MA).

2.2 Synthesis of Fe_3O_4/MPS

Fe_3O_4 nanoparticles were synthesised by the reported solvothermal reaction [18, 19]. The details of the synthesis process were as follows: first, 1.15 g of $FeCl_3 \cdot 6H_2O$, 3.20 g of NH_4Ac, 0.3424 g of sodium citrate were added to 60 ml ethylene glycol. The reaction time was 1 h at 170°C, and the colour of solution turned black. Next, it was moved to stainless-steel autoclave when cooled to room temperature. The autoclave was reacted for 8 h at 200°C. Finally, Fe_3O_4 nanoparticles were washed three times with ethanol and re-dispersed in ethanol (10 mg/ml).

To form rich double bonds on the surface of Fe_3O_4, modification of MPS was achieved. Firstly, 20 ml of ethanol, 5 ml of deionised water, 1.0 ml of $NH_3 \cdot H_2O$, and 60 µl TEOS were added to 3 ml of Fe_3O_4 suspension. Then, the mixture was magnetically stirred for 4 h at 30°C. 90 µl of MPS and 1.0 ml of $NH_3 \cdot H_2O$ was added to react overnight with magnetic stirring at 70°C. The prepared Fe_3O_4/MPS nanoparticles were washed three times with ethanol and re-dispersed in deionised water (10 mg/ml).

2.3 Synthesis of Fe_3O_4/MPS@PAA core/shell magnetic nanoparticles

The core/shell Fe_3O_4/MPS@PAA magnetic nanoparticles were synthesised in deionised water by polymerisation of AA on the surface of Fe_3O_4/MPS with TEMED and APS as the initiator. Specifically, 3 ml of Fe_3O_4/MPS dispersed in 20 ml deionised water. 150 mg of AA, 30 mg of MBA, 10 µl of TEMED, and 20 µl of APS (30 wt%) were added to the above solution. Nitrogen purged the mixture for 30 min to remove air. Then the mixture was heated to 70°C and reacted for 5 h under N_2 protection. The obtained Fe_3O_4/MPS@PAA nanoparticles were washed with ethanol and water several times, and finally suspended in deionised water (0.8 mg/ml).

2.4 Synthesis of Fe_3O_4/MPS@PAA/NTA-Ni^{2+} nanoparticles

The carboxyl group activation of nanoparticles was achieved by an EDC/NHS method. 10 ml of Fe_3O_4/MPS@PAA was activated by 30 mg of EDC and 45 mg of NHS for 1.5 h. 20 mg of NTA was added to react overnight at room temperature and collected with a magnet. The isolated Fe_3O_4/MPS@PAA/NTA magnetic nanoparticles were washed with deionised water three times and re-suspended in deionised water. Excess nickel chloride solution (0.1 M) was slowly added into the Fe_3O_4/MPS@PAA/NTA suspension to react for 1 h. Fe_3O_4/MPS@PAA/NTA-Ni^{2+} nanoparticles were washed with deionised water and re-suspended in deionised water (0.5 mg/ml).

2.5 Characterisation of magnetic nanoparticles

TEM analyses were measured by FEI Tecnai G20/JEM 2010. The size distribution and zeta potential were characterised by DLS (Malvern Zetasizer Nano ZS). Fourier transform infrared (FT-IR) spectra were measured by Nicolet IS50. XRD was characterised by X'Pert Pro from Panalytica Company. Carboxyl content was conducted by a conductivity meter (DDS-11A). The magnetic properties of nanoparticles were characterised with a vibrating sample magnetometer (VSM) from the Quantum Design Company at room temperature.

2.6 Selective binding and separation of His-tagged GFP

Ten ml of Fe_3O_4/MPS@PAA/NTA-Ni^{2+} magnetic nanoparticles (0.5 mg/ml) was collected by a magnet, washed with binding buffer (50 mM PBS buffer, 50 mM NaCl, 5 mM imidazole, pH 7.4) several times, and dispersed in 1 ml of binding buffer. 500 µl of a mixture of *E. coli* lysate (1 mg/ml) was added to incubate at room temperature for 30 min. After that, the supernatant was removed, leaving the target proteins-bound Fe_3O_4/MPS@PAA/NTA-Ni^{2+} magnetic nanoparticles. The isolated nanoparticles were rinsed with binding buffer three times to remove the non-specifically adsorbed proteins, followed by magnetic separation. Subsequently, the trapped His-tagged GFP was directly eluted from 1 ml of elution buffer (50 mM PBS buffer, 50 mM NaCl, pH 7.4) with a different imidazole concentration (250 mM, 500 mM, 1 M). All the solutions including the original solution, supernatant and eluents were collected for further analyses. The reusability of Fe_3O_4/MPS@PAA/NTA-Ni^{2+} nanoparticles was studied by six successive adsorptions and desorptions of His-tagged GFP.

His-tagged protein was purified by High-Affinity Ni-NTA Resin and Ni-NTA Magnetic Agarose Beads. Protein-bound beads were washed with 5 ml of elution buffer (50 mM PBS buffer, 50 mM NaCl, 500 mM imidazole, pH 7.4) twice. The imidazole in the eluent was removed by dialysing it against dialysis buffer (50 mM PBS buffer, pH 7.4).

Separated proteins with beads were analysed by sodium dodecyl sulphate polyacrylamide gel electrophoresis (SDS-PAGE). Fluorescence spectra were recorded with a SHIMADZU RF-6000 spectrofluorometer. The protein concentration was determined by Micro UV spectrophotometer (NANODROP 2000c, Thermo

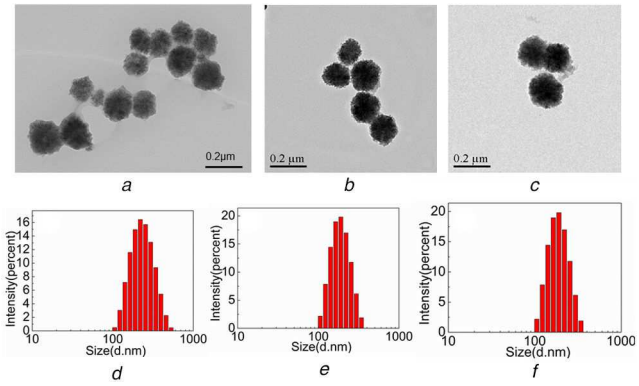

Fig. 3 *TEM images of* ***(a)*** Fe_3O_4, ***(b)*** Fe_3O_4/MPS@PAA, ***(c)*** Fe_3O_4/MPS@PAA/NTA-Ni^{2+}; The DLS results of ***(d)*** Fe_3O_4, ***(e)*** Fe_3O_4/MPS@PAA, ***(f)*** Fe_3O_4/MPS@PAA/NTA-Ni^{2+}

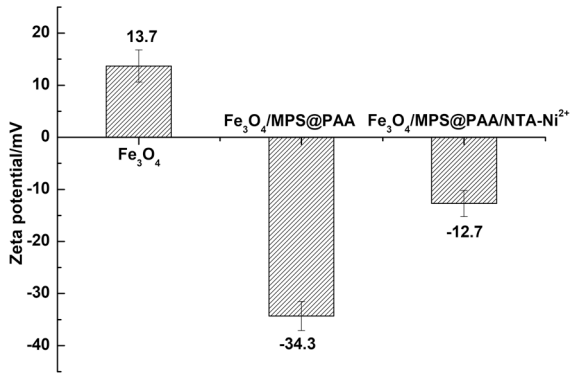

Fig. 4 *Zeta potential of Fe_3O_4, Fe_3O_4/MPS@PAA, and Fe_3O_4/MPS@PAA/NTA-Ni^{2+}*

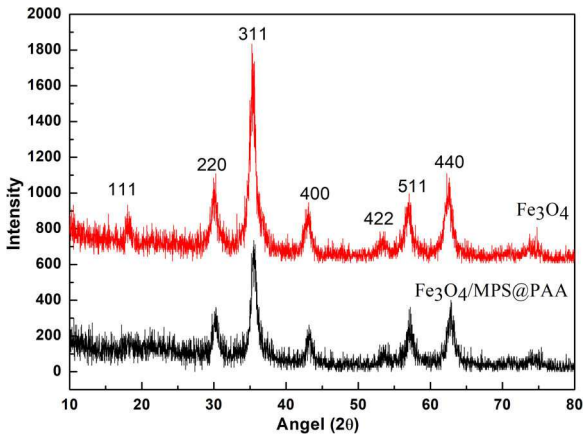

Fig. 5 *XRD patterns of Fe_3O_4 and Fe_3O_4/MPS@PAA*

Company, of US). The separation efficiency of target proteins was calculated from the following equation:

$$\text{Separation efficiency}\,(\%) = \frac{(C_1V_1 + C_2V_2 + \cdots + C_nV_n)}{C_0V_0} \times 100$$

where C_0 is the protein concentration of *E. coli* lysate, V_0 is the volume of *E. coli* lysate, $C_1, \ldots, n$ is the eluted protein concentration, and $V_{1,\ldots,n}$ is the volume of eluted protein.

The binding capacity of Fe_3O_4/MPS@PAA/NTA-Ni^{2+} was calculated according to the following equation:

$$\text{Binding capacity}\,(\text{mg/g}) = \frac{(C_1V_1 + C_2V_2 + \cdots + C_nV_n)}{m}$$

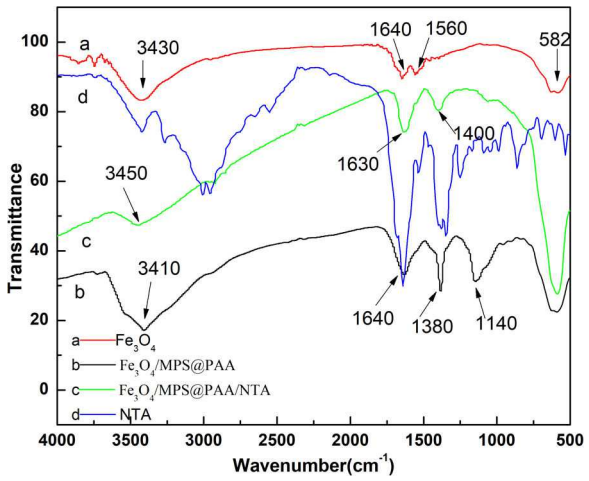

Fig. 6 *FTIR spectrum of* ***(a)*** Fe_3O_4, ***(b)*** Fe_3O_4/MPS@PAA, ***(c)*** Fe_3O_4/MPS@/PAA/NTA, ***(d)*** NTA

where $C_1, \ldots, n$ is the eluted protein concentration, $V_{1,\ldots,n}$ is the volume of eluted protein, and m is the weight of nanoparticles.

3 Results and discussion

3.1 Characterisation of magnetic nanoparticles

TEM images of Fe_3O_4, Fe_3O_4/MPS@PAA and Fe_3O_4/MPS@PAA/NTA-Ni^{2+} nanocomposites were shown in Fig. 3. The Fe_3O_4 nanoparticles were spherical and monodisperse, and had uniform size distribution with the average size of about 131.2 ± 5 nm (Fig. 3*a*). After the growth of PAA brushes, the particle diameter increased to 168 ± 5 nm obviously, indicating a ~37 nm thick polymer brushes on the surface of the Fe_3O_4 core (Fig. 3*b*). After conjugation with NTA-Ni^{2+}, the particle diameter in TEM images was ~204 ± 5 nm, which indicated that Fe_3O_4/MPS@PAA nanocomposites were coated with nearly ~36 nm thick polymer layer (Fig. 3*c*). Moreover, there was no aggregation after the modification process, presumably because of the electrostatic repulsion caused by the high negative charge of NTA. The hydrodynamic diameter (D_h) of the above-mentioned nanoparticles was in Figs. 3*d–f*, which was consistent with TEM results.

The zeta potentials for Fe_3O_4, Fe_3O_4/MPS@PAA, Fe_3O_4/MPS@PAA/NTA-Ni^{2+} nanocomposites in deionised water were shown in Fig. 4. After modification with PAA brushes, the zeta potential decreased from 13.7 to −34.3 mV, which demonstrated that a large of –COOH groups were successfully modified on the surface of Fe_3O_4 nanoparticles. The high density of –COOH groups endued the particles excellent stability because of electrostatic repulsion. After conjugation with NTA-Ni^{2+}, the zeta potential of Fe_3O_4/MPS@PAA/NTA-Ni^{2+} nanoparticles increased to −12.7 mV, indicating the success chelation of Ni^{2+}.

The crystallographic structure of the particles was further characterised by XRD. Fig. 5 performed the XRD patterns of Fe_3O_4 and Fe_3O_4/MPS@PAA nanoparticles. The diffraction peaks of Fe_3O_4 could be indexed as a face-centred cubic Fe_3O_4 phase (JCPDS card No. 19-629) [20]. The XRD pattern of Fe_3O_4/MPS@PAA was similar to that of Fe_3O_4, which indicated that the crystalline structure of nanoparticles was not affected by the modification with polymer brushes.

Fig. 6 shows the infrared spectrum of Fe_3O_4, Fe_3O_4/MPS@PAA and Fe_3O_4/MPS@PAA/NTA nanocomposites. The vibration of the Fe–O bond was at the characteristic absorption peak of 582 cm^{-1} (spectrum a) [21]. Compared with Fe_3O_4, the observed band at 1640 cm^{-1} in spectrum b was characteristic of the C = O stretching mode for the protonated carboxylate group, which subsequently took part in NTA conjugation. The peak at 1140 cm^{-1} was due to the $–CH_2$ stretching vibration presented in PAA. The peak at 3410 cm^{-1} was distinctive of –OH bonds presented in the

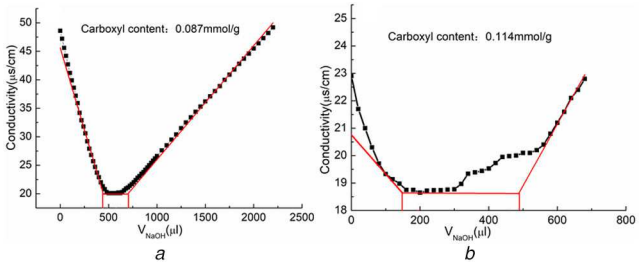

Fig. 7 *Carboxyl content of*
(a) Fe_3O_4/MPS@PAA and, ***(b)*** Fe_3O_4/MPS@PAA/NTA

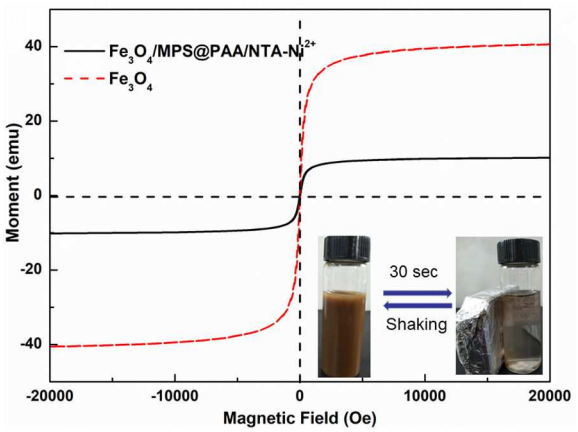

Fig. 8 *Room-temperature (300 K) magnetic hysteresis loops of nanoparticles*

PAA structure. After modification with NTA on Fe_3O_4/MPS@PAA nanoparticles, the characteristic peaks of the amide bond appeared at 3450 cm^{-1} (NH), 1630 cm^{-1} (amide I), and 1400 cm^{-1} (amide II) in spectrum c. These results confirmed the successful synthesis of magnetic nanocomposites.

The conductivity titration curve of magnetic nanoparticles (Fig. 7) provides the quantity of carboxylate content. The carboxylate content of Fe_3O_4/MPS@PAA was 0.087 mmol/g. After the reaction of Fe_3O_4/MPS@PAA with NTA, the carboxylate content was 0.114 mmol/g. These results further confirmed the polymerisation and acylation reaction in synthesis procedure.

Fig. 8 shows the magnetic hysteresis loops at room temperature ($T = 300$ K) of Fe_3O_4 and Fe_3O_4/MPS@PAA/NTA-Ni^{2+}. There were no remanence or coercivity for Fe_3O_4 and Fe_3O_4/MPS@PAA/NTA-Ni^{2+} nanoparticles, which indicated that magnetic properties could make nanocomposites susceptible to external magnetic fields (the inset in Fig. 8). The saturation magnetisation of Fe_3O_4 and Fe_3O_4/MPS@PAA/NTA-Ni^{2+} were 40.6 and 10.2 emu·g^{-1}, respectively. In comparison to Fe_3O_4 nanoparticles, the magnetisation of Fe_3O_4/MPS@PAA/NTA-Ni^{2+} nanocomposites decreased obviously because of constant surface modification, which was consistent with reports from other groups [22]. The Fe_3O_4/MPS@PAA/NTA-Ni^{2+} nanocomposites formed a brown suspension in deionised water. Under an external magnetic field, nanocomposites gathered rapidly within 1 min from their homogeneous dispersion. After removing the magnetic field, the nanocomposites rapidly re-dispersed in deionised water with slight shaking. The results showed that Fe_3O_4/MPS@PAA/NTA-Ni^{2+} nanocomposites had excellent redispersibility and magnetic responsiveness, which would facilitate the rapid protein separation.

3.2 Purification of His-tagged GFP from cell lysate

Because of the high affinity of Ni^{2+} to histidine, Fe_3O_4/MPS@PAA/NTA-Ni^{2+} nanocomposites could be used to purify His-tagged GFP in the *E. coli* cell lysate, as shown in Fig. 9. From the SDS-PAGE analysis (Fig. 9*a*), it could be seen that the

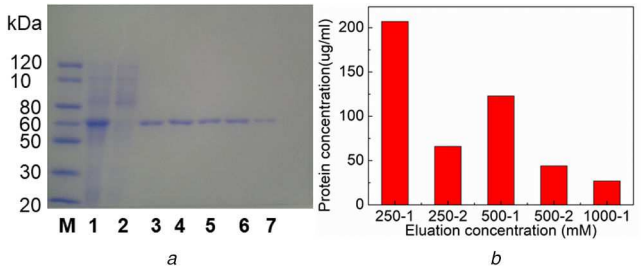

Fig. 9 *Purification of His-tagged GFP from cell lysate*
(a) SDS-PAGE analysis of purified His-tagged GFP by Fe_3O_4/MPS@PAA/NTA-Ni^{2+} nanocomposites. Lane M, the protein molecular weight marker; Lane 1, cell lysate containing His-tagged GFP; Lane 2, after treatment with Fe_3O_4/MPS@PAA/NTA-Ni^{2+}; Lanes 3–7: the fractions washed from Fe_3O_4/MPS@PAA/NTA-Ni^{2+} nanocomposites with different imidazole concentration (lanes 3 and 4, 250 mM; lanes 5 and 6, 500 mM; lane 7, 1 M), ***(b)*** Concentrations of separated proteins

molecular weight of the target proteins was 60 kD. After separated from Fe_3O_4/MPS@PAA/NTA-Ni^{2+}, there appeared an obvious single band in the elution band 3-7, with no band in the supernatant (lane 2) after treatment with Fe_3O_4/MPS@PAA/NTA-Ni^{2+}. The results showed that high specific adsorption of magnetic nanocomposites towards His-tagged GFP was achieved, and the separated proteins were pure. By quantitatively analysis of UV spectrophotometer (Fig. 9*b*), the concentrations of target proteins in the first to fifth eluents were 0.207, 0.066, 0.123, 0.044, and 0.027 mg/ml, respectively. The binding capacity of Fe_3O_4/MPS@PAA/NTA-Ni^{2+} was calculated as 93.4 mg/g, which was higher than Fe_3O_4/PMG/IDA-Ni^{2+} nanoparticles (62.0 mg/g) [17] and Ni^{2+}-IDA-GLYM@SiO_2@Mag-SiO_2 microspheres (87.4 mg/g) [8], but were lower than Fe_3O_4@Ni^{2+}-NTA-PS nanoparticles (163.52 mg/g) [23]. The results indicated that Fe_3O_4/MPS@PAA/NTA-Ni^{2+} nanoparticles exhibited high selectivity and specific enrichment for His-tagged GFP. The reason was ascribed to the modification of the PAA brushes.

Theoretically, MBA-linked PAA shell structure affects the interaction with specific proteins by the following points: (i) The PAA segments adsorb proteins by physical forces such as static electricity, hydrogen bonding, etc. [24]. (ii) Proteins are chemically adsorbed by forming amide bonds between carboxyl groups of PAA segments and amino groups on the proteins [25]. (iii) A polydentate molecule is formed by the chelating of PAA chains with metal ions (Cu^{2+}, Ni^{2+}, etc.), thus adsorbing proteins by forming complexes between metal ions and His-tagged proteins [26]. In the present system, the modification of PAA brushes on Fe_3O_4 nanoparticles greatly increased chelation sites of Ni^{2+}, and then greatly improved the coordination affinity of nanoparticles towards proteins with histidine fragments.

3.3 Comparison of purification efficiency of non-magnetic Ni-NTA, magnetic Ni-NTA and Fe_3O_4/MPS@PAA/NTA-Ni^{2+}

The binding and separating ability of non-magnetic Ni-NTA, magnetic Ni-NTA and Fe_3O_4/MPS@PAA/NTA-Ni^{2+} nanocomposites with His-tagged GFP were tested by SDS-PAGE. Lanes 3–5 (Fig. 10) show a band, which has a molecular weight of 35 kD. The intensity of the band from His-tagged GFP enriched with Fe_3O_4/MPS@PAA/NTA-Ni^{2+} nanocomposites.

His-tagged GFP protein was presented green colour under UV excitation (inset of Figs. 11*B* and *C*). The solution became colourless after incubation with magnetic Ni-NTA and Fe_3O_4/MPS@PAA/NTA-Ni^{2+} nanocomposites and the separation of His-tagged GFP-bound magnetic Ni-NTA and Fe_3O_4/MPS@PAA/NTA-Ni^{2+} from the mixture solution by using a magnet. Finally, the colour of the solution turned green again after released His-tagged GFP from magnetic Ni-NTA and Fe_3O_4/MPS@PAA/NTA-Ni^{2+} in imidazole solution. To quantify the protein separation

efficacy, we presented the fluorescent spectra of proteins in Figs. 11*A–C*. The maximum intensity of His-tagged GFP was shown at 510 nm. After incubation with Fe_3O_4/MPS@PAA/NTA-Ni^{2+}, the intensity of the fluorescent spectrum decreased with 96.3% due to the His-tagged GFP bound to Fe_3O_4/MPS@PAA/NTA-Ni^{2+}, whereas 92.7 and 94.9% decrease in the intensity of His-tagged GFP were observed after binding with non-magnetic Ni-NTA and magnetic Ni-NTA. It followed that in comparison with non-magnetic Ni-NTA and magnetic Ni-NTA, Fe_3O_4/MPS@PAA/NTA-Ni^{2+} nanocomposites could exhibit superior binding properties to the His-tagged GFP. After the release of His-tagged GFP in imidazole solution, 97.7% of His-tagged GFP was successfully released from Fe_3O_4/MPS@PAA/NTA-Ni^{2+}, whereas 85.6 and 95.4% of His-tagged GFP were released from non-magnetic Ni-NTA and magnetic Ni-NTA separately. The results showed that Fe_3O_4/MPS@PAA/NTA-Ni^{2+} nanocomposites exhibited superior separation efficiency.

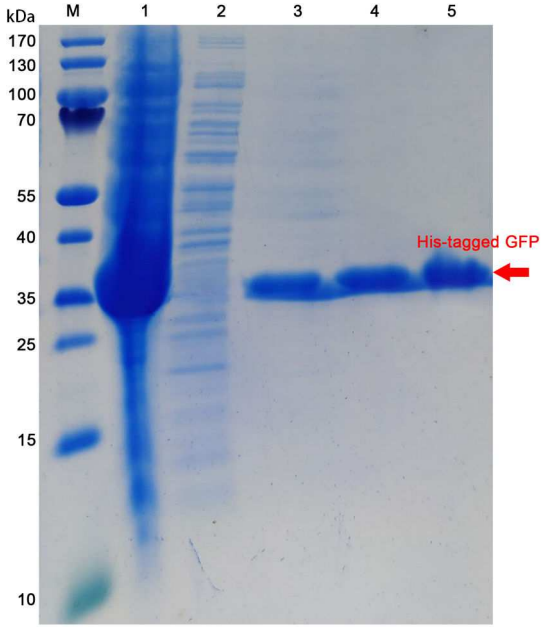

Fig. 10 *SDS-PAGE analysis of purified His-tagged GFP. Lane M: Protein MW Marker; Lane 1: stock solution of E. coli expressing His-tagged GFP; Lane 2: supernatant of extract from E. coli expressing His-tagged GFP; Lanes 3–5 are purified His-tagged GFP that purified by non-magnetic Ni-NTA, magnetic Ni-NTA and Fe_3O_4/MPS@PAA/NTA-Ni^{2+} nanocomposites, respectively*

Table 1 summarises the separation efficiency and binding capacity of non-magnetic Ni-NTA, magnetic Ni-NTA and Fe_3O_4/MPS@PAA/NTA-Ni^{2+} nanocomposites used for separation of His-tagged GFP. The binding capacity of non-magnetic Ni-NTA and magnetic Ni-NTA was lower than the 93.4 mg/g of Fe_3O_4/MPS@PAA/NTA-Ni^{2+} nanocomposites.

3.4 Reuse of Fe_3O_4/MPS@PAA/NTA-Ni^{2+} nanocomposites in His-tagged GFP separation

To test the reusability of Fe_3O_4/MPS@PAA/NTA-Ni^{2+} nanocomposites, we induced the expression of His-tagged GFP in an *E. coli* cell lysate. The Fe_3O_4/MPS@PAA/NTA-Ni^{2+} nanocomposites were incubated with cell lysate and then separated by a magnetic field. By magnetic separation and subsequent release of the captured proteins, we repeated the use of Fe_3O_4/MPS@PAA/NTA-Ni^{2+} for six times and examined the released proteins using SDS-PAGE (Fig. 12*a*). It could be seen that the His-tagged GFP was separated well by Fe_3O_4/MPS@PAA/NTA-Ni^{2+} nanocomposites up to six times, and the specificity and affinity of them remained unaffected.

The results showed that Fe_3O_4/MPS@PAA/NTA-Ni^{2+} nanocomposites had good selectivity and recyclability in the separation and purification of His-tagged protein. After six cycles of the magnetic separation and release of His-tagged GFP, the separation and efficiency were still above 90% (Fig. 12*b*), indicating that the binding capacity of Fe_3O_4/MPS@PAA/NTA-Ni^{2+} had no obvious decrease. This superior performance might be

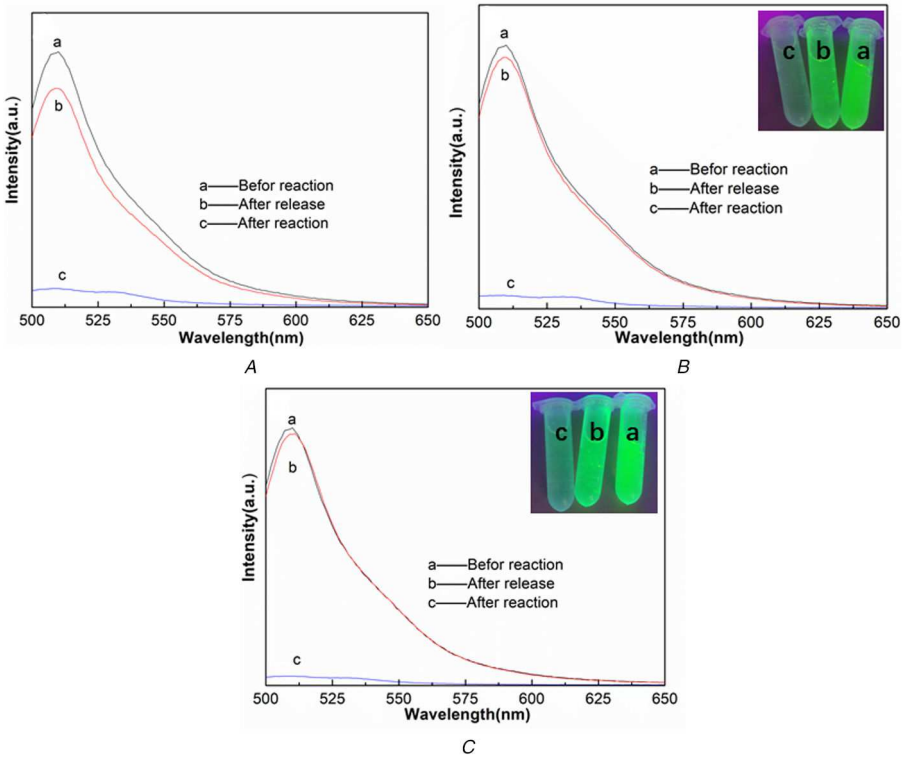

Fig. 11 *Fluorescent spectra of His-tagged GFP showing the change of emission intensity of the solution purified with* ***(A)*** Non-magnetic Ni-NTA, ***(B)*** Magnetic Ni-NTA, ***(C)*** Fe_3O_4/MPS@PAA/NTA-Ni^{2+} nanocomposites. (a) Before and (b) After reaction with beads, (c) Released His-tagged GFP in imidazole solution

Table 1 Comparison of commercially available beads that bind His-tagged GFP

Beads	Company	Separation efficiency, %	Binding capacity, mg/g
high-affinity Ni-NTA resin	GenScript	85.6	81.9
Ni-NTA magnetic agarose beads	QIAGEN	95.4	90.6
Fe_3O_4/MPS@PAA/NTA-Ni^{2+} (this work)	—	97.7	93.4

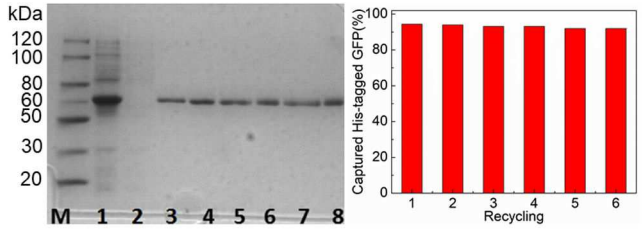

Fig. 12 *Reuse of Fe_3O_4/MPS@PAA/NTA-Ni^{2+} in His-tagged GFP separation*

(a) SDS-PAGE analysis of cell lysate containing His-tagged GFP (line 1) and proteins released from Fe_3O_4/MPS@PAA/NTA-Ni^{2+} nanocomposites reused six times (lanes 3–8). Lane M, the protein molecular weight marker; Lane 2, the supernatant after treatment with Fe_3O_4/MPS@PAA/NTA-Ni^{2+}, ***(b)*** Purification and recycling of Fe_3O_4/MPS@PAA/NTA-Ni^{2+} nanocomposites

due to multilayer binding of His-tagged protein provided by PAA brushes and magnetic cores allowing fast separation.

4 Conclusions

In this study, we used PAA brushes to encapsulate Fe_3O_4 nanoparticles and connect NTA-Ni^{2+} to prepare magnetic beads. The PAA brushes greatly increased the reaction sites for NTA-Ni^{2+}. The functionalised nanocomposites (Fe_3O_4/MPS@PAA/NTA-Ni^{2+}) were uniform with the size of 204 ± 5 nm and could be separated rapidly with saturation magnetisation of 10.2 emu·g^{-1}. These nanocomposites exhibited excellent specificity and high binding capacity (93.4 mg/g) compared with commercially available non-magnetic Ni-NTA and magnetic Ni-NTA. SDS-PAGE results showed that the separated protein was a single band with high purity. The affinity and magnetic responsiveness of Fe_3O_4/MPS@PAA/NTA-Ni^{2+} nanocomposites were maintained well after six cycles.

5 Acknowledgments

The authors thank Hubei Province Outstanding Youth Science and Technology Innovation team in institutions of higher education (T201705), the National Natural Science Foundation of China (21401051), Hubei Province Natural Science Fund Project (2014CFB595), Chutian Scholars Fund Project (2013) from the Education Department of Hubei Province, and Hundred Talents Program (2013) from the Organization Department of Hubei Province for financial support.

6 References

[1] Bray, D.: 'Protein molecules as computational elements in living cells', *Nature*, 1995, **376**, (6538), pp. 307–312

[2] Lu, W., Sun, Z., Tang, Y., *et al.*: 'Split intein facilitated tag affinity purification for recombinant proteins with controllable tag removal by inducible auto-cleavage', *Chrom. A*, 2011, **1218**, (18), pp. 2553–2560

[3] Xie, H.Y., Rui, Z., Bo, W., *et al.*: 'Fe_3O_4/Au core/shell nanoparticles modified with Ni^{2+}-nitrilotriacetic acid specific to histidine-tagged proteins', *J. Phys. Chem. C*, 2010, **114**, (11), pp. 4825–4830

[4] Xu, F., Geiger, J.H., Baker, G.L., *et al.*: 'Polymer brush-modified magnetic nanoparticles for His-tagged protein purification', *Langmuir*, 2011, **27**, (6), pp. 3106–3112

[5] Mccarthy, P., Chattopadhyay, M., Millhauser, G.L., *et al.*: 'Nanoengineered analytical immobilized metal affinity chromatography stationary phase by atom transfer radical polymerization: separation of synthetic prion peptides', *Anal. Biochem.*, 2007, **366**, (1), pp. 1–8

[6] Jian, G., Liu, Y., He, X., *et al.*: 'Click chemistry: a new facile and efficient strategy for the preparation of Fe_3O_4 nanoparticles covalently functionalized with IDA-Cu and their application in the depletion of abundant protein in blood samples', *Nanoscale*, 2012, **4**, (20), pp. 6336–6342

[7] Zhang, Y., Li, D., Yu, M., *et al.*: 'Fe_3O_4/PVIM-Ni^{2+} magnetic composite microspheres for highly specific separation of histidine-rich proteins', *ACS Appl. Mater. Interfaces*, 2014, **6**, (11), p. 8836

[8] Salimi, K., Usta, D.D., Koçer, İ., *et al.*: 'Highly selective magnetic affinity purification of histidine-tagged proteins by Ni^{2+} carrying monodisperse composite microspheres', *RSC Adv.*, 2017, **7**, (14), pp. 8718–8726

[9] Li, P., Li, L., Zhao, Y., *et al.*: 'Selective binding and magnetic separation of histidine-tagged proteins using Fe_3O_4/Cu-apatite nanoparticles', *J. Inorg. Biochem.*, 2016, **156**, (49), pp. 49–54

[10] Sahu, S.K., Chakrabarty, A., Bhattacharya, D., *et al.*: 'Single step surface modification of highly stable magnetic nanoparticles for purification of His-tag proteins', *J. Nanopart. Res.*, 2011, **13**, (6), pp. 2475–2484

[11] Wang, Y., Wang, G., Xiao, Y., *et al.*: 'Yolk–shell nanostructured Fe_3O_4@$NiSiO_3$ for selective affinity and magnetic separation of His-tagged proteins', *ACS Appl. Mater. Interfaces*, 2014, **6**, (21), pp. 19092–19099

[12] Fang, W., Chen, X., Zheng, N.: 'Superparamagnetic core–shell polymer particles for efficient purification of his-tagged proteins', *J. Mater. Chem.*, 2010, **20**, (39), pp. 8624–8630

[13] Shao, M., Ning, F., Zhao, J., *et al.*: 'Preparation of Fe_3O_4@SiO_2@layered double hydroxide core–shell microspheres for magnetic separation of proteins', *J. Am. Chem. Soc.*, 2012, **134**, (2), pp. 1071–1077

[14] Zou, X., Li, K., Zhao, Y., *et al.*: 'Ferroferric oxide/L-cysteine magnetic nanospheres for capturing histidine-tagged proteins', *J. Mater. Chem. B*, 2013, **1**, (38), pp. 5108–5113

[15] Zhou, Y., Yan, D., Yuan, S., *et al.*: 'Selective binding, magnetic separation and purification of histidine-tagged protein using biopolymer magnetic core–shell nanoparticles', *Protein Expr. Purif.*, 2018, **144**, pp. 5–11

[16] Hwang, L., Ayaz-Guner, S., Gregorich, Z.R., *et al.*: 'Specific enrichment of phosphoproteins using functionalized multivalent nanoparticles', *J. Am. Chem. Soc.*, 2015, **137**, (7), pp. 2432–2435

[17] Zhou, Y., Yuan, S., Liu, Q., *et al.*: 'Synchronized purification and immobilization of his-tagged β-glucosidase via Fe_3O_4/PMG core/shell magnetic nanoparticles', *Sci. Rep.*, 2017, **7**, p.41741

[18] Zhang, Y., Yu, M., Zhang, C., *et al.*: 'Highly selective and ultrafast solid-phase extraction of N-glycoproteome by oxime click chemistry using aminooxy-functionalized magnetic nanoparticles', *Anal. Chem.*, 2014, **86**, (15), pp. 7920–7924

[19] Xue, X., Wang, B., Xi, X., *et al.*: 'Polymer decorated magnetite materials as smart protein separators to manipulate the high loading of heme proteins', *New J. Chem.*, 2015, **39**, (7), pp. 5735–5742

[20] Ghandoor, H.E., Zidan, H.M., Khalil, M.M.H., *et al.*: 'Synthesis and some physical properties of magnetite (Fe_3O_4) nanoparticles', *Int. J. Electrochem.*, 2012, **7**, (6), pp. 5734–5745

[21] Wang, Y., Shen, Y., Xie, A., *et al.*: 'A simple method to construct bifunctional Fe_3O_4/Au hybrid nanostructures and tune their optical properties in the near-infrared region', *J. Phys. Chem. C*, 2010, **114**, (32), pp. 4297–4301

[22] Fried, T., Shemer, G., Markovich, G.: 'Ordered two-dimensional arrays of ferrite nanoparticles', *Adv. Mater.*, 2010, **13**, (15), pp. 1158–1161

[23] Jose, L., Lee, C., Hwang, A., *et al.*: 'Magnetically steerable Fe_3O_4@Ni^{2+}-NTA-polystyrene nanoparticles for the immobilization and separation of his6-protein', *Eur. Polym. J.*, 2019, **112**, pp. 524–529

[24] Wittemann, A., Haupt, B., Ballauff, M.: 'Adsorption of proteins on spherical polyelectrolyte brushes in aqueous solution', *Phys. Chem. Chem. Phys.*, 2003, **5**, (8), pp. 1671–1677

[25] Dong, R., Krishnan, S., Baird, B.A., *et al.*: 'Patterned biofunctional poly (acrylic acid) brushes on silicon surfaces', *Biomacromolecules*, 2007, **8**, (10), pp. 3082–3092

[26] Cullen, S.P., Liu, X., Mandel, I.C., *et al.*: 'Polymeric brushes as functional templates for immobilizing ribonuclease A: study of binding kinetics and activity', *Langmuir*, 2008, **24**, (3), pp. 913–920